Physical Disturbance Rejection Methods in Myokinetic Control of Prosthetic Limbs

Flavia Paggetti, Marta Gherardini, Valerio Ianniciello, Simone Cirelli, and Christian Cipriani, *Senior Member, IEEE*

Abstract*—*Objective: **The myokinetic control interface for limb protheses involves implanting small permanent magnets in the residual muscles of the stump, retrieving their displacement induced by muscle contraction using external magnetic sensors, and mapping such displacements to motor commands. We have previously shown the feasibility of tracking several magnets implanted in an anatomically relevant workspace. However, to clinically translate the interface, strategies to address different kinds of external disturbances compromising its functioning are mandatory. Among these, physical disturbances, viz. relative displacement between the sensors and the magnets not due to voluntary contraction, could significantly hinder the interface usability.** ***Methods:*** **Here we propose three rejection methods sought to mitigate this problem: one aims to realign the sensors and the magnets when a disturbance is detected, through numerical approximation methods; the others exploit differential measurements. We applied these concepts to upper limb prostheses, by mimicking the presence of physical disturbances in simulations and through a physical setup, reproducing four target muscles of a human forearm to be potentially implanted. Finally, we evaluated the rejection ability of one of those methods during the first-in-human implementation of the myokinetic interface.** ***Results:*** **All methods proved capable of rejecting the disturbances, showing median localization errors below 10% the displacement undergone during contraction.** ***Conclusion:*** **Results suggest that the optimal rejection method is application-specific, and provide hints for assessing different factors influencing the best choice.** ***Significance:*** **Other than being crucial for the myokinetic interface development, these outcomes also provide interesting insights for many biomedical applications exploiting remote magnetic tracking.**

***Index Terms*—Human-machine interface, magnetic tracking, myokinetic interface, physical disturbances, prosthetics.**

I. Introduction

IN THE last decades magnetic tracking has been proposed for many applications in bioengineering [1], [2], [3], [4]. The transparency of the human body to low-frequency magnetic fields represents indeed an intriguing property for intra-body applications, as it allows to wirelessly record signals generated by (magnetic) devices inside the body. We transferred this concept to the field of assistive devices, in particular prosthetic control, by introducing in 2016 what we called *myokinetic control interface* [5], [6]. This approach involves implanting small permanent magnets into the residual muscles of the stump and tracking their displacement using magnetic field sensors housed within the prosthetic socket. Unlike state of art control interfaces exploiting electrical signals collected from the muscle during contraction, the myokinetic control interface retrieves the *physical displacement* of the muscle and translates such information into control signals for the assistive device or prosthetic limb.

The myokinetic interface emerges together with several innovative approaches proposed over the past 20 years for controlling prosthetic hands [7]. These approaches aim to develop technologies and surgical techniques that allow a direct interaction with the natural control sources (i.e., muscles or nerves), to derive selective control signals with reduced noise and cross-talk effects. For example, wireless implantable electrodes like IMES [8], [9] or epimysial electrodes in combination with osseointegrated percutaneous implants [10], [11] have been proposed to collect muscle electromyographic (EMG) signals. Both solutions demonstrated improved functionality and reliability compared to standard-of-care surface electrodes, although they introduce the need to either implant wireless components requiring a power demanding transcutaneous energy transfer, or wired components with a percutaneous feedthrough, which imply higher hygienic care, respectively. In contrast, the compact size of the magnets (cylinders with a volume $\sim$1/7 that of IMES) allows for a minimally invasive implantation in the small muscles of the forearm [12], and does not require cables or power supply.

In spite of such attractive features, the measurement of an intra-body signal (i.e., the magnet position) from an external source (i.e., magnetic field sensors on the skin) suffers from

Received 19 September 2024; revised 12 December 2024; accepted 26 January 2025. Date of publication 30 January 2025; date of current version 27 June 2025. This work was supported in part by the European Research Council under the MYTI Project under Grant ERC-2023-PoC, in part by the Italian Ministry of Research, under the complementary actions to the PNRR "Fit4MedRob - Fit for Medical Robotics" under Grant PNC0000007, and in part by the Centro Protesi – Istituto Nazionale per L'Assicurazione Contro Gli Infortuni Sul Lavoro through NoProblem Project under Grant PR23-CR-P3. *(Corresponding author: Christian Cipriani.)*

Flavia Paggetti, Marta Gherardini, and Valerio Ianniciello are with the BioRobotics Institute, Scuola Superiore Sant'Anna, Italy, and also with the Department of Excellence in Robotics and AI, Scuola Superiore Sant'Anna, Italy.

Simone Cirelli is with the Scuola Superiore Sant'Anna, Italy.

Christian Cipriani is with the BioRobotics Institute, Scuola Superiore Sant'Anna, 56127 Pisa, Italy, and also with the Department of Excellence in Robotics and AI, Scuola Superiore Sant'Anna, 56127 Pisa, Italy (e-mail: christian.cipriani@santannapisa.it).

Digital Object Identifier 10.1109/TBME.2025.3536854

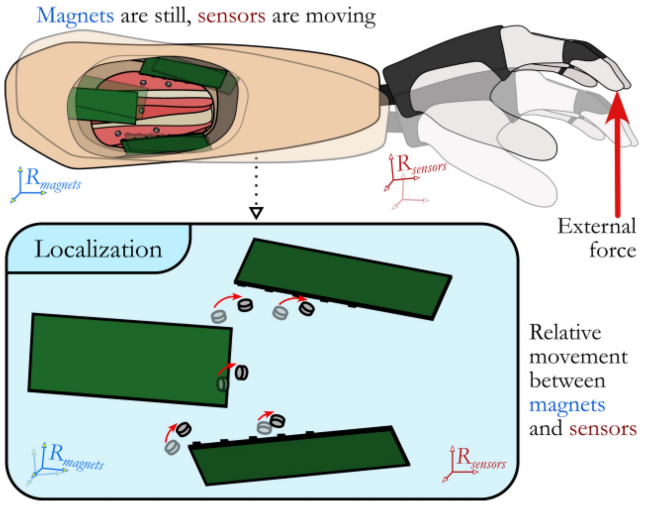

Fig. 1. Myokinetic interface and movement artifacts. Representative example of the effect of external loads on the multi-magnet localizer. The load induces a displacement of the socket, and thus of the sensors, relative to the residual limb (upper panel). As a consequence, a displacement of the magnets not caused by muscle contraction, and thus by the user's intention, is detected (lower panel).

artifacts due to relative movements between the two systems [13]. Indeed, as the sensing apparatus of a myokinetic interface is integrated within and jointly liable with the prosthetic socket, any movement of the latter relative to the stump may result in an artifact of magnet displacement (i.e., of muscle contraction) (Fig. 1). Such artifact, if not mitigated, could result in improper activations of the prosthetic limb, reducing the system robustness and undermining the user's confidence in controlling it.

Here, we investigate the efficacy of different solutions in counteracting artifacts induced by undesired magnet-to-sensors movements. Specifically, we identified a realistic implant configuration (i.e., a forearm with four residual muscles available and different number of magnets implanted) and we simulated/produced movement artifacts by applying simultaneous translations and rotations to an external sensor array, considering plausible ranges of disturbances which could affect the socket in realistic scenarios. Under such conditions, we compared the response of three different methods designed to compensate for movement artifacts, and to increase the robustness of the interface. The first method involves monitoring the displacement of one magnet per muscle (as in previous works [5], [14], [15]), and an optimization-based strategy that derives the *Roto-Translation Matrix* compensating for the sensor relative movements (*RTM* method). Differently, the other two methods (*One Reference Magnet - 1RM* method, and *Two Magnets per Muscle - 2MM* method, respectively) rely on the immunity of differential measurements from common-mode disturbances.

The three methods were first compared by simulating the implantation and displacement of the magnets into the muscles using a 3D CAD model (simulated setup) and a physical mockup (on bench setup) of the forearm. Finally, the viability of the 2MM method to reject disturbances was further assessed during a specific case study of one trans-radial amputee receiving implanted magnets and wearing the prosthetic socket (clinical setup). While the theoretical foundation of the methods, along with the simulation and on bench results, has clear implications for all amputation levels and anatomical regions, the clinical setup provides specific guidelines for implementing the myokinetic interface in trans-radial upper limb subjects.

While the obtained outcomes do not indicate a general superiority of any of the three methods, they suggest that the preferred method should be based on different factors, such as computational cost [15], amputation level and stump anatomy [16], and main direction of muscle deformation [13].

II. Materials and Methods

A. Localization Algorithm and Disturbance Rejection Methods

The *myokinetic* control interface is based on the online estimation of the pose of magnets (i.e., localization of their position and orientation in space) which are implanted in residual contractile muscles. The localization data is then mapped to the contractile state of the muscles to build output signals, used to command the several degrees of freedom in a robotic assistive device, like a prosthetic hand.

In this study, the poses of the magnets were tracked using a multi-magnet localization algorithm, based on the Levenberg Marquard Algorithm [17] and already validated in earlier studies [5], [15]. The algorithm was implemented in Matlab (MathWorks, Natick, MA) (for the simulated setup), and on an embedded platform (on bench and clinical setup) [15]. The three proposed disturbance rejection methods were applied to the output of our multi-magnet localization algorithm (Fig. 2).

B. Roto-Translation Matrix Method – RTM

The displacement of individual magnets is monitored with respect to an initial/rest position and the degree/direction of unintended magnet-to-sensor movements are estimated. To detect these movements, the approach relies on a magnet trajectory (defined by a set of 3D points $\boldsymbol{t_i}$), registered in absence of disturbances, named calibration trajectory (Fig. 2(b)). Practically, this trajectory could be derived by asking the amputee to contract the implanted muscles, with the limb at rest and no applied load. A cylinder of a set radius $d_{\max}$ is computationally built around this trajectory to define a region in which the magnet is expected to travel. When a localized current position $\boldsymbol{p}$ of any of the magnets exceeds the boundaries of this region (hence, an external disturbance is detected), the (4 x 4) transformation matrix $\mathbf{T}$ that solves the following system:

$$\min_i \left(\|\boldsymbol{t_i} - \boldsymbol{T}\boldsymbol{p}\|\right) < d_{max} \tag{1}$$

is used to realign the magnets along the calibration trajectories. According to this method, a possible output signal s to be used for controlling the prosthetic limb, is the *realigned* relative displacement of each magnet from its rest position.

$$s = \|\boldsymbol{T}\boldsymbol{p} - \boldsymbol{p}^{\boldsymbol{rest}}\| \tag{2}$$

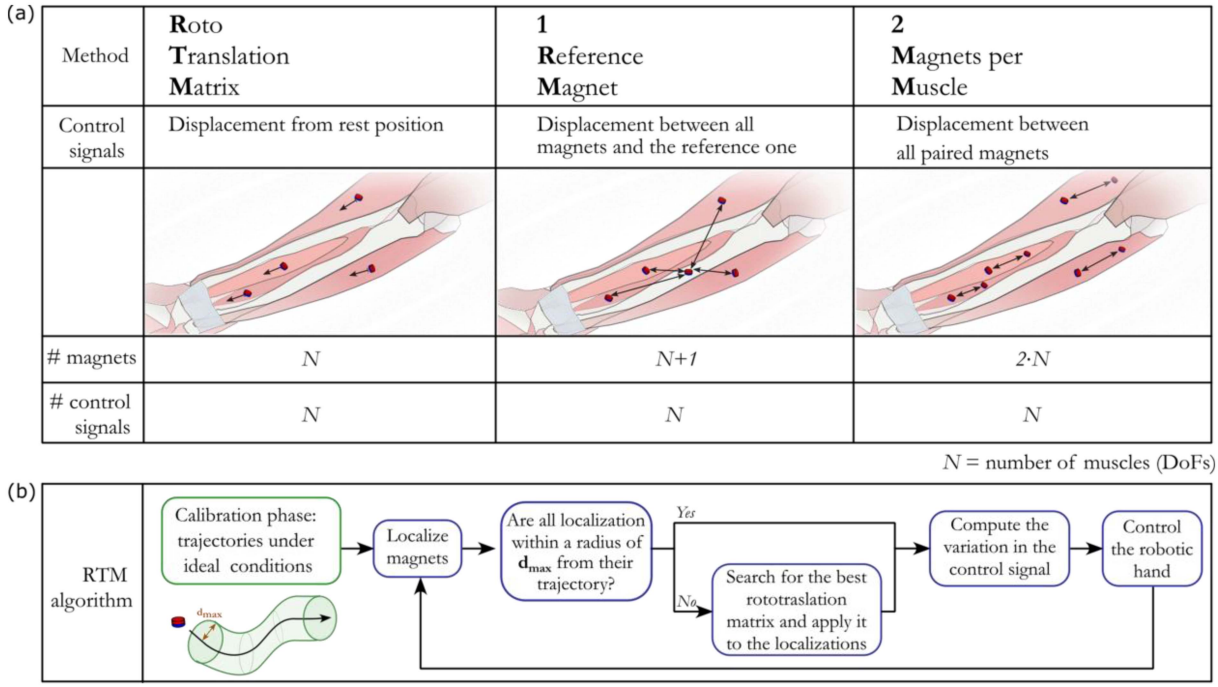

Fig. 2. Disturbance rejection methods. (a) Details on the different rejection methods, including the outcome measure (i.e., control signal), number of magnets and control signals per each method. (b) Workflow of the *RTM* rejection method implementation, involving: (i) calibration phase, (ii) definition of the $d_{\max}$ parameter, (ii) application of the numerical approximation method when disturbances are detected.

Therefore, for *N* implanted magnets, *N* is the number of available control signals. When considering the magnet orientation, a similar control signal can be computed by substituting the magnet position **p** with the magnet orientation **v**.

C. One Reference Magnet Method – 1RM

The displacement of individual magnets is monitored with respect to a reference magnet, located on a fixed anatomical site (e.g., a bone), akin to [18]. Therefore, this approach involves implanting an additional magnet with respect to the target ones in the muscles. The approach relies on the assumption that external disturbances would physically affect all muscles/magnets in the same manner, namely generating the same kind of disturbance-induced displacement on all magnets. Consequently, differential measurements like the control signal employed by this method will remain unaffected by these common mode inputs. The displacement between each moving magnet and the reference magnet is the output signal s.

$$s = \|\boldsymbol{p} - \boldsymbol{p}_{reference}\| \tag{3}$$

For *N* magnets, *N-1* control signals are available.

D. Two Magnets Per Muscle Method – 2MM

The relative displacement between magnets is monitored via differential measurements, as in [13], [19]. The approach involves implanting two magnets per muscle and monitoring their relative displacement (i.e., intra-muscle displacement), which is the output signal. The approach relies on the assumption that external disturbances would physically affect both paired magnets in the same manner, inducing a common mode displacement that can be filtered out by employing differential measurements between the magnet pairs.

$$s = \|\boldsymbol{p}_{magnet1} - \boldsymbol{p}_{magnet2}\| \tag{4}$$

For *N* magnets, *N/2* control signals are available.

E. Simulated and On Bench Setup

1) Simulated Setup: Aided by a 3D CAD model we simulated a representative case of an amputation at the trans-radial level [13], [16] with four residual muscles receiving implanted magnets (Fig. 3(a)): the abductor pollicis longus (APL), the flexor pollicis longus (FPL), the first compartment of the extensor digitorum (ED-I), and the first compartment of the flexor digitorum profundus (FDP-I). Ideally, this set of muscles would allow to control the index and the thumb independently, including thumb abduction, of a prosthetic hand.

Magnets were modeled as NdFeB with a remanent magnetization Br = 1.27T, and a 2 mm radius and height. The magnetic field produced by the magnets was computed using an analytical model for cylindrical magnets, as in [20], [21], and was sampled on a grid of 480 sites (uniform distribution, 12° angular distance, 10 mm far from the axial direction) arranged around the residual limb, simulating the presence of three-axis sensors [16], [22].

Each of the selected muscle was virtually implanted with one (moving) or two (one moving and one still) magnets, based on the rejection method being investigated. The muscle contraction was mimicked by displacing moving magnets, one at a time, along 15 mm long trajectories discretized into 11 steps

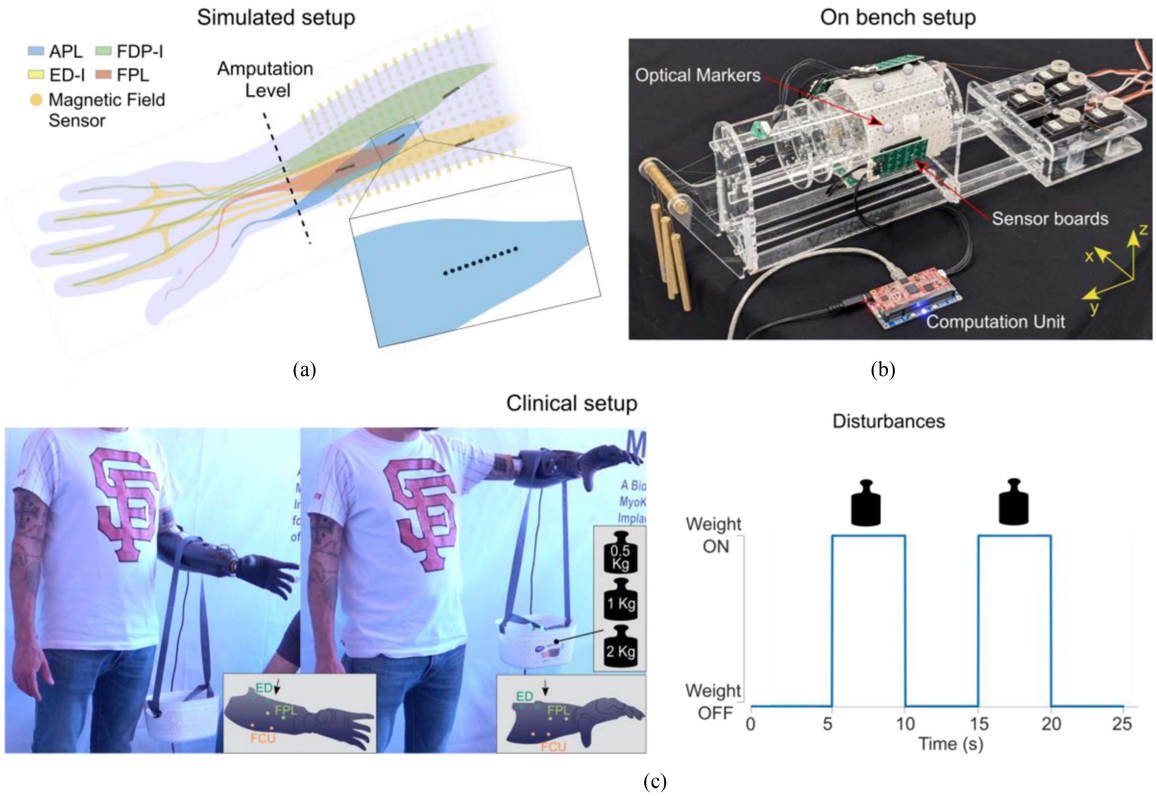

Fig. 3. Simulated (a), On Bench (b) and Clinical (c) setup and applied artifacts. (a) Four muscles received the implant, namely the abductor pollicis longus (APL), the flexor pollicis longus (FPL), the first compartment of the extensor digitorum (ED-I), and the first compartment of the flexor digitorum profundus (FDP-I). The figure shows the 3D CAD model used to simulate the implants, the selected muscles, the sensor array, and the trajectories imposed to the four moving magnets. (b) On bench setup composed of the forearm mockup, the acquisition units and the embedded computation unit. Four optical markers were placed on the external frame to reconstruct the applied movement artifacts. (c) Clinical study involving one amputee in two arm positions (shoulder abduction – flexed elbow and shoulder adduction – flexed elbow). The figure on the right shows the timing of the load application.

(Fig. 3(a)). Trajectories involved both an axial (d_a) and a radial (d_r) displacement component, according to a contraction model described in [22]. In the resting (un-contracted) position, the magnetic moment vectors pointed radially towards the nearest sensor, vice versa during contraction the moving magnets tilted [22]. At each step, the magnetic field generated by the magnets was computed and the magnet poses were estimated through the multi-magnet localization algorithm. [21], [20], [16], [22].

Muscle contractions were first simulated without the presence of physical disturbances (control condition) and then by generating physical disturbances on the sensor grid (test condition). The physical disturbances were mimicked by means of: (i) translations along the y-axis (aligned with the arm) in the range ± 6 mm, as it is likely the most affected in real-world conditions; (ii) rotations around the y-axis in the range $\pm 15°$; (iii) rotations around the x- and z-axis in the range $\pm 10°$. To simulate realistic conditions, each artifact was linearly increased/decreased in successive steps, and all disturbances were applied simultaneously. Consequently, individual translations along the x- and z- axes were not separately assessed, as their effects were inherently included in the combined disturbance scenario.

Implementation of RTM: When implementing the RTM method, one magnet was implanted along the centerline of each muscle, 35 mm distally to the proximal musculotendinous junction, with implantation depths of 28 mm, 24 mm, 31 mm, and 10 mm for APL, FPL, FPD-I, and ED-I, respectively. During the calibration phase each magnet was moved along its trajectory, simulating muscle contraction, and localized at each step. The retrieved poses were stored and used to build the cylinder of radius d_{max} (Fig. 2(b)). The magnet movement along the trajectory was thus repeated under disturbed conditions and at each step, the magnet poses were checked. If at least one magnet was localized outside of its volume, the corrective measure was applied, using the fmincon Matlab function (algorithm = 'spq', StepTolerance/FunctionTolerance = 10^{-12}, MaxFunEvals = 2000). Realigned magnet localizations were finally computed. The cylinder radius d_{max} was set to 100μm, roughly corresponding to the localizer precision [14], [15], so that even the smallest artifacts were detected.

Implementation of 1RM: When implementing the 1RM approach, one reference magnet was placed in the center of the forearm to approximate its placement on a bone (e.g., the ulna), in addition to the four magnets implanted in RTM.

Implementation of 2MM: To implement the *2MM* method a total of eight magnets were virtually implanted. Specifically, in addition to the four magnets used for the *RTM* approach, one additional magnet was placed in each target muscle, at an initial distance of 35 mm from the first magnet, right below the

proximal musculotendinous junction, where the displacement caused by contraction could be neglected [22]. This condition allowed to maximize the relative displacement between paired magnets in the same muscle, i.e., the output (or control) signal for this configuration.

2) On Bench Setup: The simulated configurations (*RTM, 1RM, 2MM*) were essentially replicated using a mockup of the human forearm [5], [15], [23] (Fig. 3(b)). Magnets were attached to wires mimicking the target muscles (APL, FPL, ED-I, FDP-I), pulled by servomotors to simulate muscle contraction. The reference magnet of *1RM* and the non-moving magnets of *2MM* were attached to the mockup frame at a site approximating their target position, namely the bone and the proximal musculotendinous junctions of the muscles (∼35 mm apart from the moving magnet), respectively.

Eight sensor boards already used in [15] (20 three-axial magnetic sensors on each board, inter-sensor distance of 9 mm) were mounted on a frame arranged around the forearm mockup (Fig. 3(b)). Data acquired by the sensor boards were transmitted to a computation unit that performed online localization, [15], as in [12]. One servomotor per time was used to displace each magnet along its trajectory in 11 discrete steps, as in the simulations, while continuously localizing the magnet poses. Given the available hardware, an output frequency of 38 Hz, 36 Hz and 16 Hz could be achieved for *RTM*, *1RM*, and *2MM* respectively (the localization rate is inversely proportional to the number of magnets).

Physical disturbances were manually applied to the frame accommodating the sensor boards, and subsequently quantified by a three-camera 6DoF optical tracking system (V120:Trio, OptiTrack, US) working at 120 Hz, ensuring sub-millimetric resolution (Fig. 3(b)). Overall, translations of ±15 mm were applied along the mockup axis, simultaneously with rotations in the range of those applied in simulation (Fig. 3(b)).

F. Error Metrics

The position and orientation errors E were computed according to the following formula:

$$E = s^{actual} - s$$

where s^{actual} represents the control signal of a method (either accounting for the position or orientation) computed with the actual (not localized) magnet poses. For the simulated and on bench setups the error E was assessed in terms of model (e_m) and cross-talk (e_{ct}) error, as in [5]. e_m refers to inaccuracies in retrieving the displacement of the moving magnet, while e_{ct} refers to false predictions of simultaneous displacements detected for the steady ones. The orientation error was not assessed for the on bench setup data as the actual rotation of the magnets could not be properly controlled and measured along the trajectory. We considered a localization error in position acceptable if it was below 10% the range of the control signal (e.g., length of the magnet trajectory). This threshold would enable the implementation of control algorithms that map varying degrees of muscle contraction (i.e., magnet displacement) to the prosthetic movement, with good resolution. Similarly, for the orientation error the acceptability threshold was set to 9° (10% the right angle), according to previous works [14].

The above-mentioned errors were compared across rejection methods, using the Kruskal-Wallis test with Bonferroni correction ($\alpha \sim = 0.02$), after checking the normality of data distribution (Kolmogorov-Smirnov Test).

G. Clinical Setup

One participant with a transradial amputation received the implantation of six permanent magnets in three muscles of the residual forearm (two magnets per muscle – *2 MM* method), namely ED, FPL, and the flexor carpi ulnaris (FCU). This test was conducted as part of a larger study investigating the feasibility and safety of the myokinetic interface through a temporary implant of six weeks [12]. All experimental procedures were carried out at the AOUP hospital (Azienda Ospedaliero Universitaria Pisana). The study was approved by the Ethical Committee of AOUP and the Italian Ministry of Health. Consent to publish identifiable images of research participants was obtained from the participant and notified to the competent authorities.

The participant was fitted with a self-contained prosthesis which integrated seven sensor boards and the computation unit inside a prosthetic socket, and a MIA robotic hand (Prensilia Srl, Italy) (Fig. 3(c)). To investigate the effect of physical disturbances on the accuracy of the localizer, we cyclically loaded the socket with a mass (5 seconds loaded and 5 seconds unloaded, 4 repetitions). Specifically, we tested the effects of three loads (0.5 kg, 1 kg, and 2 kg) on the prosthetic socket while the participant was maintaining a static posture with the arm positioned in two configurations: elbow flexed at 90 degrees and the shoulder (i) fully adducted, or (ii) abducted at 90 degrees (Fig. 3(c)). During this test the participant was instructed to maintain the muscles relaxed to prevent displacement of the magnets caused by voluntary contractions.

Localization data were recorded at 42 Hz and stored for offline analysis via a dedicated PC application.

The actual displacement induced by the physical disturbance (load condition) was quantified by measuring the variation in the control signal s (4) for the *2MM* approach (localized displacement between magnet pairs) with respect to the rest state of the muscle:

$$\Delta s_{2MM} = s - s^{rest} \tag{5}$$

for each loading of the socket, and then averaged across repetitions of the same load. To evaluate the intensity of the disturbance itself and the effectiveness of the disturbance-rejection method, we also computed the displacement induced by the external load on each individual magnet:

$$\Delta s_{individual} = \|\boldsymbol{p} - \boldsymbol{p}^{\boldsymbol{rest}}\| \tag{6}$$

aggregating the result of the two individual magnets of the same muscle. For both measures (Δs and $\Delta s_{individual}$), the rest configuration was updated throughout the acquisitions, to compensate for the muscle hysteresis. Finally, statistical comparison between Δs and $\Delta s_{individual}$ was performed through the Wilcoxon rank-sum test.

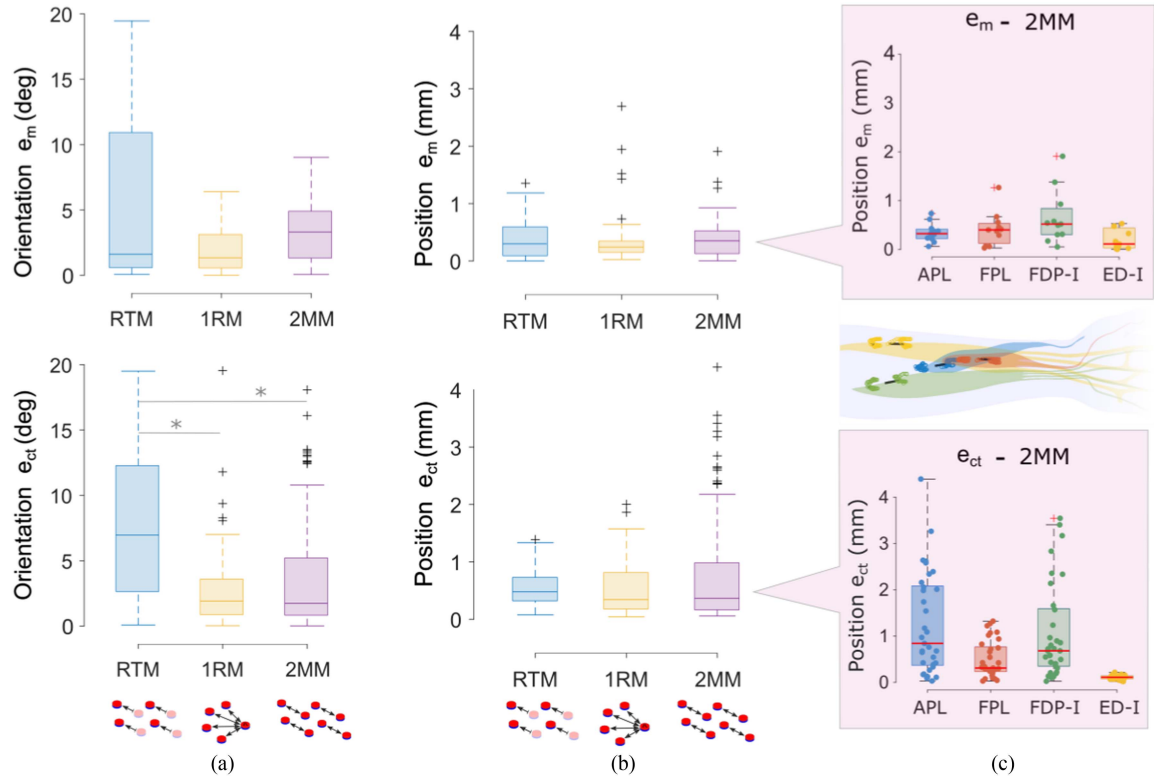

Fig. 4. Orientation and positions errors from the simulated setup for all corrective methods. Boxplots depict localization errors - (a) orientation and (b) position - in terms of both e_m and e_{ct}, aggregated across all magnets for the different rejection methods. (c) Representative results showing the position errors (model, e_m, and cross talk, e_{ct}) obtained with the 2MM method for each magnet pair, i.e., each muscle. The 3D CAD on the right depicts the output of the localization when disturbances are applied (for simplicity, non moving magnets are not reported).

III. Results

The combined effects of external disturbance and the movement of different magnets influenced localization outcome. Notably, all data series were found to be non-normally distributed, with outliers and increased localization errors linked to moving magnets located farther from the sensors.

A. Simulated Setup

The three methods proved capable of rejecting the applied disturbances, as demonstrated by the median value of the aggregated errors across magnets, that proved always below 0.45 mm for position and <7deg for orientation, for both e_m and e_{ct} (Fig. 4(a) and (b), achieved over a trajectory length of 15 mm and an overall rotation of 25°. In general, for the position e_m and e_{ct} and for the orientation e_m, results proved not statistically different. Differently, the orientation e_{ct} for *RTM* demonstrated statistically worse than the other methods, with an e_{ct} ranging between 2.96 deg and 12.29 deg (25th and 75th percentile).

A deeper analysis associated to the individual muscles is presented for the *2MM* method (Fig. 4(c)). For all magnet pairs, e_m proved below 0.52 mm, i.e., 3.5% the magnet trajectory length. The largest e_m, equal to 1.91 mm, was obtained for the magnets in FDP-I, i.e., those that exhibited the largest distance from the sensors (∼31 mm), while the remaining magnet pairs showed e_m values always below 1.27 mm. Accordingly, magnets in FDP-I and in APL (∼28 mm depth) showed larger e_{ct} compared to the other magnet pairs. In particular, their e_{ct} ranged between 0.37 mm and 2.08 mm for APL, between 0.35 mm and 1.59 mm for FDP-I (25th and 75th percentile), and reached peaks of 4.39 mm and 3.55 mm, respectively. Nevertheless, their median e_{ct} proved equal to 5.6% and 4.5% of the magnet trajectory, respectively. The lowest errors were achieved for the magnets in ED-I (∼10 mm depth), showing a median e_{ct} of 0.11 mm. This correlation between depth of the magnets and the localization errors was found also for the *RTM* method but not for *1RM* (not shown).

B. On Bench Setup

Looking at the aggregated outcomes across magnets, as for the simulation results, all methods proved capable of rejecting the disturbances, achieving median e_m values below 1.11 mm and e_{ct} values below 0.78 mm (Fig. 5(b)), over a trajectory length of ∼15 mm. *1RM* proved statistically better than both *RTM* and *2MM* for e_{ct} and better than *2MM* in terms of e_m. Finally, *2MM* performed statistically worse than both the other methods for e_m, with 25th and 75th percentile error values equal to 0.59 mm and 2.14 mm (3.9% and 14.3% the trajectory length, respectively).

As for the simulations, the position errors associated to each muscle of the *2MM* method are presented in detail (Fig. 5(b)). Once more, a correlation between magnet-to-sensor distance

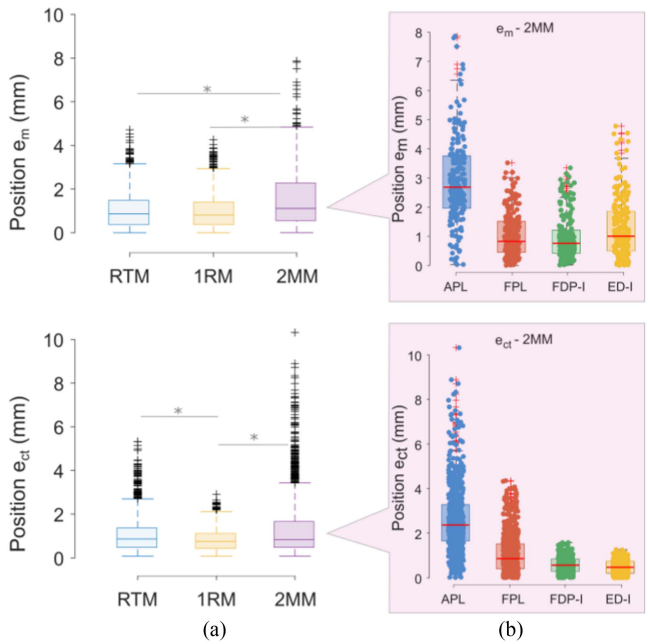

Fig. 5. Position errors from the on bench setup for all corrective methods. (a) Representative result showing the position error (model, e_m, and cross talk, e_{ct}) obtained with the 2MM method for each magnet pair, i.e., each muscle. (b) Boxplots depict localization errors (position and orientation) in terms of both e_m and e_{ct}, aggregated across all magnets for the different rejection methods ($*$ indicates significant difference according to the Kruskal-Wallis test with Bonferroni correction).

and localization errors was found; however, the magnet-to-sensor distances in the physical mockup and the simulated scenario were marginally different. Larger errors were obtained for the magnets in APL ($\sim$40 mm depth), with e_m ranging between 1.95 mm (25th percentile, 13% the trajectory length) and 3.74 mm (75th percentile, 24.9%), and e_{ct} ranging between 1.65 mm (25th percentile, 11%) and 3.32 mm (75th percentile, 22.1%). The magnet pairs in FPL, FDP-I and ED-I (37 mm, 25 mm and 21 mm depth, respectively), showed e_m between 0.41 mm (25th percentile) and 1.83 mm (75th percentile), corresponding to 2.7% and 12.2% the magnet trajectory length. Finally, e_{ct} ranged between 0.21 mm (25th percentile, 1.4%) and 1.50 mm (75th percentile, 10%), with median values of 0.86 mm, 0.57 mm, and 0.47 mm for FPL, FPD-I, and ED-I, respectively. Differently, considering both *RTM* and *1RM* rejection methods, localization errors proved largely comparable across magnets/magnet pairs (not shown).

C. Clinical Setup

The applied load generated a variation in the control signal Δs and on the individual magnet displacement $\Delta s_{individual}$ that varied between $<$0.01 mm and 1.8 mm depending on the amount of load and the arm position (Fig. 6).

In both positions and for all loads (except for the FCU muscle under 1 kg mass with abducted shoulder), the variation in control signal (displacement between magnet pairs) Δs proved always statistically lower than the displacement induced on individual magnets $\Delta s_{individual}$ by external loads. Notably, the amount of this displacement mainly depended on the muscle, and not on the load intensity. Indeed, the load effects on the FCU muscle were minimal, resulting in median Δs ($\Delta s_{individual}$) ranging between 0.04 mm (0.11 mm) and 0.22 mm (0.24 mm) across positions and load intensities. Differently, FPL and ED showed higher Δs ($\Delta s_{individual}$) in both positions, with median values ranging between 0.05 mm (0.37 mm) and 0.34 mm (0.46 mm) for FPL and 0.05 mm (0.22 mm) and 0.19 mm (0.54 mm) for ED.

Finally, as the average displacement caused by voluntary contraction was of $\sim$2 mm, $\sim$3 mm and $\sim$1 mm for magnet pairs in ED, FPL and FCU [12], respectively, the displacement induced by the external loads Δs proved generally $<$10% such control signals, akin to the outcomes achieved with the simulated and on bench setups.

IV. Discussion

This study compared three methods (*RTM*, *1RM* and *2MM*) for rejecting movement artifacts that could compromise the usability and robustness of a myokinetic control interface. The effects of potential disturbances were replicated in an anatomically relevant environment (i.e., an amputated human forearm), both in simulations and through a physical mockup. In addition, we presented the preliminary in-human validation of the *2MM* method, showing its ability to mitigate the effect of loads applied to the prosthetic socket. The simulation setup enabled a fine control of the system parameters, such as magnet position, orientation and trajectories, facilitating a comprehensive evaluation of the performance of each method under ideal conditions. The on bench set up served to increase the realism of the study by assessing errors arising from a combination of factors, including electrical noise, hardware components and the reduced number of sensors. Although magnet trajectories could be controlled with lower resolution, results effectively assessed errors caused solely by physical disturbances, without considering possibly related changes in magnet trajectory/muscle displacement. On the contrary, the influence of these aspects could be preliminary assessed in the clinical scenario, that introduced additional variables not accounted for in the previous setups, including changes in muscle length during varying arm positions and the effects of loads on the muscle.

Overall, all methods effectively compensated for the applied disturbances, with average localization errors consistently below 10% the length of the trajectory undergone by the magnets during contractions. While the obtained outcomes do not indicate a general superiority of any of the three methods, differences in performance may be attributed to intrinsic features of the methods.

First, each method tested a different number of magnets, while it is known that localization accuracy decreases with the number of magnets [24]. However, this study did not aim to standardize the methods based on magnet count; rather, the focus was on aligning them according to the number of available control sources, i.e., in this case, the number of available muscles. Hence, we selected a realistic implant configuration, e.g., a forearm with four (eligible) residual muscles, and implemented

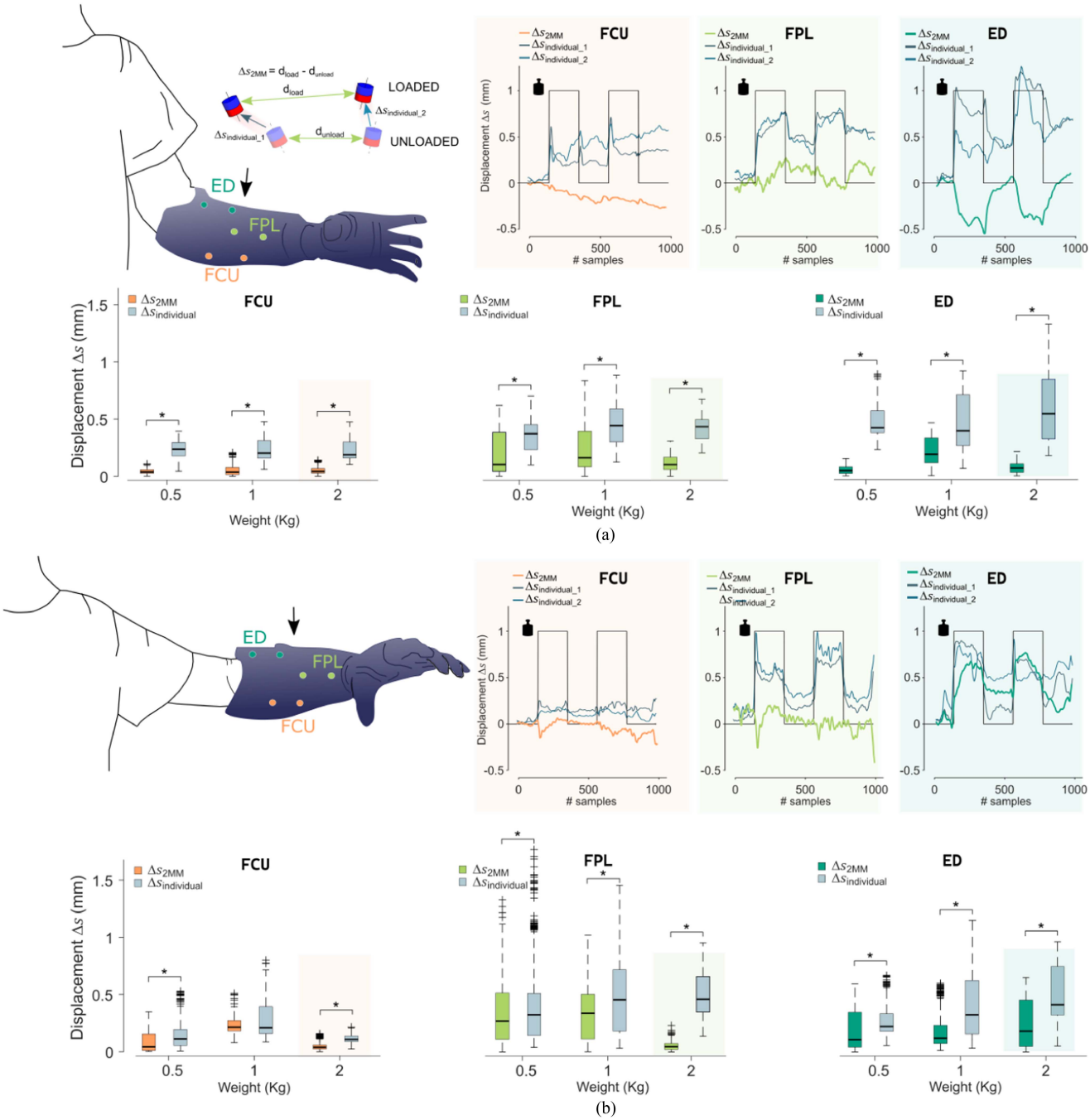

Fig. 6. Load-induced displacement from the clinical implementation of the 2MM method. (a) Results show the effect of different weights applied on the socket (weight direction represented by the black arrow) on the displacement of the magnet pairs Δs_{pair} and of the individual magnets $\Delta s_{\text{individual}}$, for the three target muscles (ED, FPL, FCU). On the upper part of the figure, a representative example (two repetitions) of displacement through time is reported, for the magnet pair and the individual magnets, when a 2Kg-mass is applied. Results are shown for two positions, namely adducted shoulder - flexed elbow (a), and abducted shoulder - flexed elbow (b). Statistically significant differences are displayed ($*$: $p<0.05$).

such methods accordingly. Given this, the larger localization errors of *2MM* (Fig. 5) are not surprising, since: (i) the number of magnets was (almost) doubled compared to the other methods, and (ii) the tracking errors of the paired magnets summed up (as for *1RM*) [13]. Despite a few outliers with higher error values, such as the magnets implanted in the APL, the median error across magnets consistently remained within the acceptable threshold.

We believe that the larger orientation errors achieved by *RTM* (Fig. 4(a)) are due to the specific formulation of the cost function used to correct for the sensor movements. In fact, when an artifact is detected, i.e., at least one magnet deviates beyond d_{max} from its intended trajectory, the cost function tries to minimize this distance, while neglecting orientation. To effectively exploit magnet orientation as a control signal for the prosthesis, the cost function should be tailored to minimize both the distance and the

relative orientation of the magnets with respect to the calibration trajectory.

While *2MM* (Fig. 4(c) and Fig. 5(b) and *RTM* (not shown) showed larger localization errors for magnets implanted at deeper sites (APL ad FDP-I), in agreement with previous findings [14], [16], this pattern was not observed in *1RM*. This discrepancy arises because 1RM measures the displacement between magnet pairs located at different sites. Specifically, being the reference magnet located far from the sensors (i.e., on the bone), its larger localization error influences the accuracy of all control signals, thus cancelling out significant differences between magnets/sites.

In the clinical setup the uneven distribution of the load-induced displacement across different muscles (Fig. 6) is likely attributed to the site of load application, specifically the area of the forearm where the rope was tethered. Indeed, for both arm positions the magnets experiencing higher load-induced displacements (ED and FPL) were located directly below the rope anchorage (Fig. 6). Additionally, we hypothesize that the hysteresis experienced by most of the magnets after the first loading of the socket (Fig. 6 upper panels) is due to the combined effects of tissue viscoelasticity [25] and an initial socket adjustment, resulting in an initial magnet-to-sensor shift. Finally and unexpectedly, the almost constant load-induced displacement regardless of the load intensity (Fig. 6) suggests that the localization errors induced solely by external loads are lower than anticipated. Nonetheless, while this preliminary evaluation focused on the two extreme positions in which the participant could sustain a load, future work should investigate multiple limb positions and various points of load application to better reflect daily life scenarios.

Given these considerations, it is clear that the selection of the appropriate method will depend on the specific application and the residual anatomy involved. Specifically, with short stumps or multiple muscles available, maintaining the necessary inter-magnet and magnet-to-sensor distances to ensure accurate localization becomes increasingly challenging [14], [16]. Therefore, in these conditions the 2MM method may require selecting a limited number of exploitable control signals. Conversely, computing the displacement between magnet pairs implanted in the same muscle would enable a direct measure of muscle length and velocity, allowing to accurately correlate muscle activation to muscle force [26]. Notably, this information could be integrated with data from other sensing technologies explored for prosthetic control, such as ultrasound and EMG, to develop more complex and accurate neuromusculoskeletal models [27], [28]. While muscle kinematics could also be derived from the displacement of individual magnets from rest (*RTM*) or by mapping the displacement of a magnet relative to a reference one (*1RM*), it is known that measuring multiple points (*2MM*) provides a more accurate and comprehensive representation of muscle behavior [29].

Here, we simulated the magnet displacement along the muscle centerline, thus constrained to a straight line joining the paired magnets in the *2MM* case. However, when a muscle shows large radial displacements, the *2MM* method would inevitably detect smaller displacement ranges [13]. This principle applies to all cases where the displacement between magnet pairs is measured, viz. also *1RM*, thus the main direction of muscle deformation should be carefully considered when selecting the rejection method. In contrast, the *RTM* method allows to exploit the full range of muscle displacement. Nonetheless, the lack of a differential measure requires the implementation of a numerical approximation method whenever a disturbance is detected, in addition to the one needed to retrieve the magnet poses. This requirement introduces issues related to computation time and hardware resource utilization, which needs to be carefully evaluated on a case-by-case basis. As far as the computation time is concerned, a tradeoff could be defined between the number of times the correction algorithm is applied and the desired localization accuracy, by tuning the threshold value ($d_{\max}$) employed to detect the artifacts.

Finally, 1RM minimizes the number of magnets needed to reject movement artifacts without requiring additional computation, but at the cost of additional surgery to attach a magnet to the bone. Contrary to the simplified assumption here, this magnet would not remain stationary, but would move during pronation and supination. This could be leveraged to restore rotational proprioception, as suggested in [30]. Simultaneously, the control signal could be updated by calibrating the position of the reference magnet during pronation/supination, and adjusting the displacement of the other magnets accordingly.

Considering these factors, we selected the 2MM method for clinical implementation, despite its slightly higher localization errors, as we deemed it the most reliable and informative control strategy for the myokinetic interface at this stage. Our goal was to assess the feasibility of monitoring individual muscle displacement by implanting magnets in the muscle, as approved by the ethical committee, which led to the exclusion of the 1RM method. Furthermore, implanting more magnets allowed to better characterize the overall muscle behavior. In addition, the greater computational and hardware demands of the RTM method led us to select the 2MM method for the first proof-of-concept. Interestingly and ancillary, during the in-human implant [12] computing differential measures proved beneficial also for compensating unwanted magnet displacements caused by the so-called limb position effect [31], [32]. Future implants should consider the efficacy of a specific method in compensating both types of disturbances, taking into account all considerations and trade-offs made above. Finally, the efficacy of algorithms and compensation strategies should always be contextualized with the surgical setting: if advanced surgical techniques increase the range of magnet displacement, as shown in [33], the effect of physical disturbances could be largely mitigated.

V. Conclusion

In all setups, the three methods (*RTM*, *1RM* and *2MM*) effectively reduced artifacts caused by undesired magnet-to-sensors movements. However, the selection of the most appropriate method will ultimately depend on the specific requirements of the application. *RTM* and *2MM* should be preferred when a biomimetic control strategy is sought, if hardware resources,

computation time and stump length are compatible with their implementation. If these conditions are not met, *1RM* would allow to exploit the intrinsic capability of differential measurements to reject common mode noise with fewer magnets and would provide useful bone-orientation information that could be integrated in the control loop.

References

[1] A. M. Franz et al., "Electromagnetic tracking in medicine—A review of technology, validation, and applications," *IEEE Trans. Med. Imag.*, vol. 33, no. 8, pp. 1702–1725, Aug. 2014, doi: 10.1109/TMI.2014.2321777.

[2] C. Hu et al., "Locating intra-body capsule object by three-magnet sensing system," *IEEE Sensors J.*, vol. 16, no. 13, pp. 5167–5176, Jul. 2016, doi: 10.1109/JSEN.2016.2558198.

[3] L. Maréchal et al., "Design optimization of a magnetic field-based localization device for enhanced ventriculostomy," *J. Med. Devices*, vol. 10, no. 1, 2016, Art. no. 011006, doi: 10.1115/1.4032614.

[4] A. Yang et al., "A new tracking system for three magnetic objectives," *IEEE Trans. Magn.*, vol. 46, no. 12, pp. 4023–4029, Dec. 2010, doi: 10.1109/TMAG.2010.2076823.

[5] S. Tarantino et al., "The myokinetic control interface: Tracking implanted magnets as a means for prosthetic control," *Sci. Reports*, vol. 7, no. 1, 2017, Art. no. 17149, doi: 10.1038/s41598-017-17464-1.

[6] S. Tarantino et al., "A myokinetic HMI for the control of hand prostheses: A feasibility study," *Biosyst. Biorobotics*, vol. 15, pp. 575–579, 2016, doi: 10.1007/978-3-319-46669-9_95/COVER.

[7] D. Farina et al., "Toward higher-performance bionic limbs for wider clinical use," *Nature Biomed. Eng.*, vol. 7, no. 4, pp. 473–485, 2023, doi: 10.1038/s41551-021-00732-x.

[8] P. F. Pasquina et al., "First-in-man demonstration of a fully implanted myoelectric sensors system to control an advanced electromechanical prosthetic hand," *J. Neurosci. Methods*, vol. 244, pp. 85–93, 2015.

[9] R. F. Weir et al., "Implantable myoelectric sensors (IMESs) for intramuscular electromyogram recording," *IEEE Trans. Biomed. Eng.*, vol. 56, no. 1, pp. 159–171, Jan. 2009, doi: 10.1109/TBME.2008.2005942.

[10] M. Ortiz-Catalan, B. Håkansson, and R. Brånemark, "An osseointegrated human-machine gateway for long-term sensory feedback and motor control of artificial limbs," *Sci. Transl. Med.*, vol. 6, no. 257, pp. 257re6–257re6, 2014, doi: 10.1126/scitranslmed.3008933.

[11] M. Ortiz-Catalan et al., "A highly integrated bionic hand with neural control and feedback for use in daily life," *Sci. Robot.*, vol. 8, no. 83, Oct. 2023, Art. no. eadf7360, doi: 10.1126/SCIROBOTICS.ADF7360.

[12] M. Gherardini et al., "Restoration of grasping in an upper limb amputee using the myokinetic prosthesis with implanted magnets," *Sci. Robot.*, vol. 9, 2024, Art. no. 3260.

[13] F. Paggetti et al., "To what extent implanting single vs pairs of magnets per muscle affect the localization accuracy of the myokinetic control interface? Evidence from a simulated environment," *IEEE Trans. Biomed. Eng.*, vol. 70, no. 10, pp. 2972–2979, Oct. 2023, doi: 10.1109/TBME.2023.3272977.

[14] M. Gherardini et al., "Localization accuracy of multiple magnets in a myokinetic control interface," *Sci. Reports*, vol. 11, no. 1, 2021, Art. no. 4850, doi: 10.1038/s41598-021-84390-8.

[15] V. Ianniciello, M. Gherardini, and C. Cipriani, "Transcutaneous magnet localizer for a self-contained myokinetic prosthetic hand," *IEEE Trans. Biomed. Eng.*, vol. 71, no. 3, pp. 1068–1075, Mar. 2024, doi: 10.1109/TBME.2023.3325910.

[16] S. Milici et al., "The myokinetic control interface: How many magnets can be implanted in an amputated forearm? Evidence from a simulated environment," *IEEE Trans. Neural Syst. Rehabil. Eng.*, vol. 28, no. 11, pp. 2451–2458, Nov. 2020, doi: 10.1109/TNSRE.2020.3024960.

[17] H. P. Gavin, *The Levenberg-Marquadt Method For Nonlinear Least Squares Curve-Fitting Problems*. Durham, NC, USA: Duke Univ., 2024.

[18] M. Gherardini et al., "Feasibility study on disentangling muscle movements in TMR patients through a myokinetic control interface for the control of artificial hands," *IEEE Robot. Automat. Lett.*, vol. 7, no. 3, pp. 7240–7246, Jul. 2022, doi: 10.1109/LRA.2022.3181748.

[19] C. R. Taylor et al., "Magnetomicrometry," *Sci. Robot.*, vol. 6, 2021, Art. no. 0656.

[20] N. Derby and S. Olbert, "Cylindrical magnets and ideal solenoids," *Amer. J. Phys.*, vol. 78, no. 3, pp. 229–235, Mar. 2010, doi: 10.1119/1.3256157.

[21] A. Caciagli et al., "Exact expression for the magnetic field of a finite cylinder with arbitrary uniform magnetization," *J. Magnetism Magn. Materials*, vol. 456, pp. 423–432, Jun. 2018, doi: 10.1016/J.JMMM.2018.02.003.

[22] M. Gherardini, A. Mannini, and C. Cipriani, "Optimal spatial sensor design for magnetic tracking in a myokinetic control interface," *Comput. Methods Programs Biomed.*, vol. 211, 2021, Art. no. 106407, doi: 10.1016/j.cmpb.2021.106407.

[23] S. P. Mendez et al., "Data-driven real-time magnetic tracking applied to myokinetic interfaces," *IEEE Trans. Biomed. Circuits Syst.*, vol. 16, no. 2, pp. 266–274, Apr. 2022, doi: 10.1109/TBCAS.2022.3161133.

[24] S. Tarantino et al., "Feasibility of tracking multiple implanted magnets with a myokinetic control interface: Simulation and experimental evidence based on the point dipole model," *IEEE Trans. Biomed. Eng.*, vol. 67, no. 5, pp. 1282–1292, May 2020.

[25] Y. C. Fung, *Biomechanics: Mechanical Properties of Living Tissues Second Edition*, 2nd ed. Berlin, Germany: Springer, 1993.

[26] G. T. Yamaguchi, *Dynamic Modeling of Musculoskeletal Motion: A Vectorized Approach for Biomechanical Analysis in Three Dimensions*. Berlin, Germany: Springer, 2005.

[27] X. Yang et al., "Ultrasound as a neurorobotic interface: A review," *IEEE Trans. Syst., Man, Cybern., Syst.*, vol. 54, no. 6, pp. 3534–3546, Jun. 2024, doi: 10.1109/TSMC.2024.3358960.

[28] M. Sartori et al., "Robust simultaneous myoelectric control of multiple degrees of freedom in wrist-hand prostheses by real-time neuromusculoskeletal modeling," *J. Neural Eng.*, vol. 15, no. 6, Oct. 2018, Art. no. 066026, doi: 10.1088/1741-2552/AAE26B.

[29] B. van Hooren, P. Teratsias, and E. F. Hodson-Tole, "Ultrasound imaging to assess skeletal muscle architecture during movements: A systematic review of methods, reliability, and challenges," *J. Appl. Physiol.*, vol. 128, no. 4, pp. 978–999, Apr. 2020, doi: 10.1152/JAPPLPHYSIOL.00835.2019.

[30] E. J. Rouse et al., "Development of a model Osseo-Magnetic Link for intuitive rotational control of upper-limb prostheses," *IEEE Trans. Neural Syst. Rehabil. Eng.*, vol. 19, no. 2, pp. 213–220, Apr. 2011, doi: 10.1109/TNSRE.2010.2102365.

[31] C. Cipriani et al., "The effects of weight and inertia of the prosthesis on the sensitivity of electromyographic pattern recognition in relax state," *JPO, J. Prosthetics Orthotics*, vol. 24, no. 2, pp. 86–92, 2012.

[32] N. Jiang et al., "Effect of arm position on the prediction of kinematics from EMG in amputees," *Med. Biol. Eng. Comput.*, vol. 51, no. 1/2, pp. 143–151, Feb. 2013, doi: 10.1007/S11517-012-0979-4.

[33] M. Daliri et al., "The second clinical study investigating the surgical method for the kineticomyographic control implementation of the bionic hand," *Sci. Reports*, vol. 13, no. 1, Dec. 2023, Art. no. 18387, doi: 10.1038/s41598-023-45578-2.